Single and multiple Auger decay processes from the Ne^+ $1s^{-1}2p^{-1}np$ shake-up states studied with a multielectron coincidence method

Y. Hikosaka,[1] T. Kaneyasu,[2] P. Lablanquie,[3] F. Penent,[3] and K. Ito[4]
[1]*Graduate School of Medicine and Pharmaceutical Sciences, University of Toyama, Toyama 930-0194, Japan*
[2]*SAGA Light Source, Tosu 841-0005, Japan*
[3]*Sorbonne Université, UPMC, Université Paris 06, Centre National de la Recherche Scientifique, Laboratoire de Chimie Physique-Matière et Rayonnement (UMR 7614), 4 place Jussieu, 75252 Paris Cedex 05, France*
[4]*Photon Factory, Institute of Materials Structure Science, Tsukuba 305-0801, Japan*

(Received 29 November 2017; published 5 February 2018)

The single, double, and triple Auger decay processes from the $1s^{-1}2p^{-1}np$ shake-up states of Ne have been studied with a multielectron coincidence method. It is revealed that the Rydberg electron promoted in the initial photoionization step generally acts as a spectator both in the single and double Auger decays. The single Auger decay predominantly produces three-hole one-particle final states while leaving the Rydberg electron virtually unchanged. In the cascade double Auger paths, the Rydberg electron is a spectator in the first step of the cascade process but is subsequently released in the second step, leading to the formation of three-hole final states. The direct paths of double Auger decays, which are much weaker than the cascade paths, produce preferably four-hole one-particle states due to the spectator behavior of the Rydberg electron. The distributions of the Ne^{4+} states populated by the triple Auger decays are also presented.

DOI: 10.1103/PhysRevA.97.023405

I. INTRODUCTION

The inner-shell photoelectron spectra of atoms and molecules exhibit satellite structures at lower kinetic energy than the main core-hole peaks [1]. These satellite structures are due to core-electron ejection accompanied by the promotion of a valence electron into an unoccupied orbital, corresponding to the formation of core-hole states with an excited electron. Such photoionization processes can be interpreted generally by the shake-up mechanism [2].

Auger decay is one of the important decay pathways of the shake-up states, similar to the main core-hole states. Characteristic of the Auger decay from the shake-up states is the behavior of the promoted electron in the initial photoionization step. This can play a crucial role in determining the populations of Auger final states. For the Auger decay processes emitting a single Auger electron, the participation of the promoted electron, which either fills the core hole or is ejected toward the continuum, can lead to the formation of a doubly charged state with two holes ($2h$) in the valence orbitals. On the other hand, if the promoted electron is not involved in the decay process but is retained in the outer orbital, a three-hole one-particle ($3h1e$) final state can be produced. Such states are rarely populated by decay from the main core-hole state.

Besides single Auger decay, double Auger decay in which two Auger electrons are emitted can sizably contribute to the total Auger intensity of shake-up states. For example, double Auger decay contributes 21% to the total Auger decay from the Ar $2p$ shake-up states [3]. The two Auger electrons can be ejected simultaneously (i.e., by the direct double Auger path) or in a stepwise way by the creation and the decay of an intermediate doubly charged state (i.e., the cascade double Auger path). By analogy to single Auger decay, the direct double Auger path can be categorized further by the behavior of the promoted electron. While the participation of the electron can lead to the formation of a three-hole ($3h$) triply charged state, a four-hole one-particle ($4h1e$) state should also be formed when the promoted electron fully acts as a spectator to the process.

Conventional Auger spectroscopy has provided only partial information on the Auger decay of shake-up states even for the single Auger processes, because the Auger structures are easily hidden behind the intense Auger transitions from the main core-hole states. Isolation of the Auger structures associated with the shake-up states can be achieved by coincidence detection of the Auger electrons with the photoelectrons emitted at the formations of the shake-up states [4]. In practice, spectra of the single Auger decays from molecular shake-up states have been obtained by electron coincidence spectroscopy, showing the preference of the spectator processes [5–8]. As for double Auger decay, the cascade paths from shake-up states of Ne $1s$ [9] and Ar $2p$ [3] have been clarified by multielectron coincidence spectroscopy, and the characteristic property of the final states populated by direct double Auger paths in an open-shell oxygen molecule was discussed very recently [7].

In the present work, we have investigated the single and multiple Auger decay processes from the Ne $1s$ shake-up states by multielectron coincidence spectroscopy, in order to gain, for this benchmark case, a complete view of the decay mechanism relevant to the behavior of the promoted electron. The different Auger decay paths studied in this work are summarized in Fig. 1. Conventional Auger spectroscopy has located complex Auger lines associated with the shake-up states and assigned them to the single Auger decays into $3h1e$ levels [10]. The present coincidence study clarifies the predominant formations of the $3h1e$ states in the single

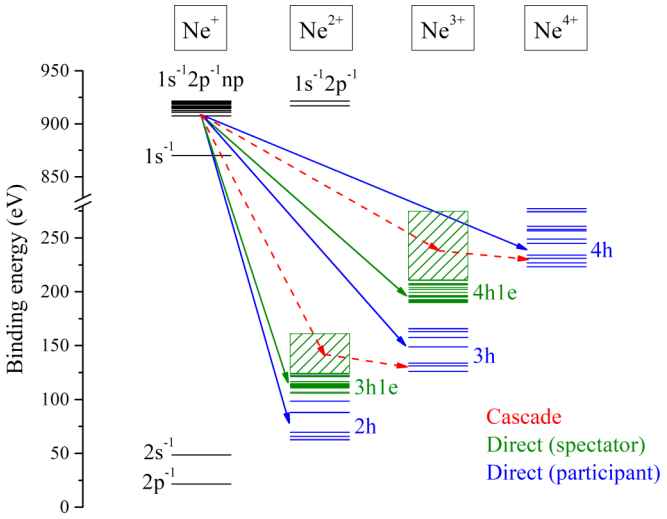

FIG. 1. Energy level diagram for Ne ions. Different Auger decay paths from Ne 1*s* shake-up state are presented.

Auger decays, implying that the promoted electron strongly prefers the spectator behavior at the single Auger emissions. In contrast, the dominant formation of the $3h$ states resulting from the participation of the Rydberg electron is observed in the total double Auger decays. This results from the strong cascade path whose intermediate $3h1e$ states were partially assigned in our previous work [9]. However, by masking the cascade paths, it is found that $4h1e$ states, retaining the Rydberg electron, are predominantly formed in the direct double Auger paths. The present observations demonstrate that the electron promoted in the initial photoionization step behaves almost exclusively as a spectator in the first step of all decay paths of the core hole. If the subsequent decay of the formed states are energetically allowed, this involves the Rydberg electron as a participant and constitutes cascade paths.

II. EXPERIMENT

The experiment was performed at the undulator beamline BL-16A of the Photon Factory. The storage ring was operated in the single bunch mode under top-up injection. Synchrotron radiation was monochromatized by a grazing incidence monochromator using a varied-line-spacing plane grating. A mechanical chopper [11] was used in order to block a certain fraction of the light pulses, thereby allowing the light pulse period to be stretched to 12.5 μs. Multielectron coincidence spectroscopy was performed by using a magnetic bottle electron spectrometer whose description is given elsewhere [11,12]. Conversion of the electron time of flight to kinetic energy was achieved by measuring Ar photoelectron spectral lines at different photon energies. The uncertainty of the electron kinetic energy, resulting from the calibration, is less than the energy resolution ΔE of the spectrometer. The energy resolving power of the spectrometer, $E/\Delta E$, was estimated to be nearly constant at 60 for electrons of $E > 3$ eV, though ΔE was limited to around 20 meV [full widrth at half maximum (FWHM)] for $E < 1$ eV. The measured detection efficiency decreases slowly with electron kinetic energy from $75 \pm 5\%$ ($E \approx 0$ eV) to $40 \pm 5\%$ ($E \approx 800$ eV). The detector dead time

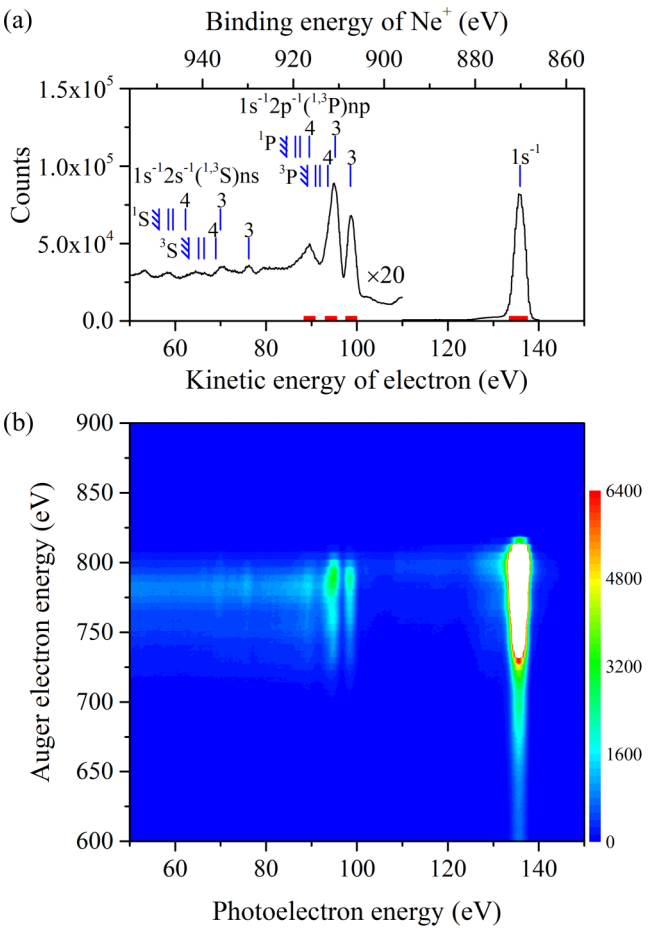

FIG. 2. (a) Photoelectron spectrum derived from the total events in the coincidence dataset accumulated at a photon energy of 1006 eV for Ne. The locations of the 1*s* main and shake-up satellite states [13] are indicated with vertical bars. The four kinetic-energy ranges set to extract the curves in Figs. 3(a)–3(d) are marked in red. (b) Two-dimensional map showing energy correlation between photoelectrons in the same range as in (a) and Auger electrons in the kinetic-energy range of 600–900 eV. Color represents number of coincidences found in a box of a 1 eV (vertical) × 0.37 eV (horizontal) size.

of 15 ns prevented detection of electrons with close energies. A multielectron coincidence dataset was accumulated for Ne at a photon energy of 1006 eV with a photon bandwidth of around 2 eV. The accumulation time was 12 h, with a count rate around 3 kHz.

III. RESULTS AND DISCUSSION

A. Single Auger decay

The photoelectron spectrum derived from the total events in the coincidence dataset, which is shown in Fig. 2(a), exhibits a 1*s* photoelectron peak at a kinetic energy of ~136 eV and shake-up satellite structures in the kinetic-energy range below 100 eV. Most of the shake-up states lying in 85–100 eV have the configurations of $1s^{-1}\,2p^{-1}\,(^{1,3}P)np$ [13], resulting from the promotion of a $2p$ valence electron into an np Rydberg orbital. The convergence limits of the $2p$ promotion are the thresholds of the core-valence ionization (or shake-off process)

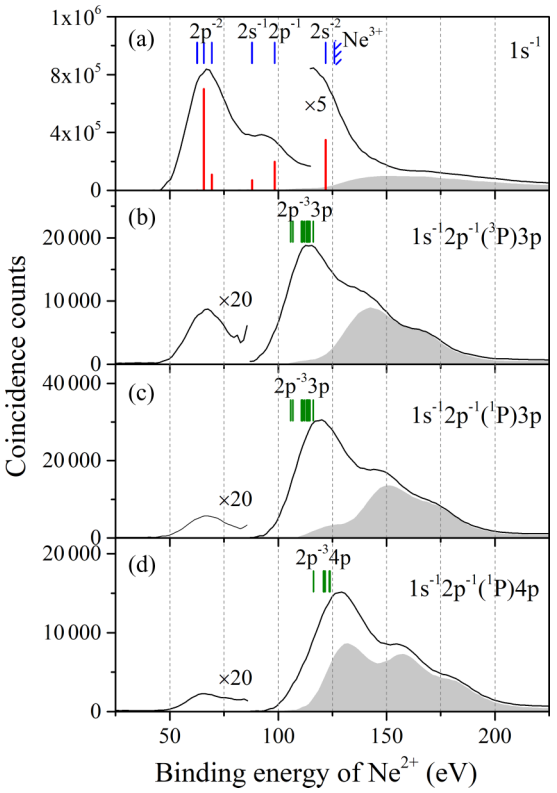

FIG. 3. Auger electron spectra (black solid) obtained in coincidence with photoelectrons for the formations of (a) $1s^{-1}$, (b) $1s^{-1}\,2p^{-1}\,(^3P)3p$, (c) $1s^{-1}\,2p^{-1}\,(^1P)3p$, and (d) $1s^{-1}\,2p^{-1}\,(^1P)4p$. Contributions from $1s^{-1}\,2p^{-1}\,(^3P)4p$ and $1s^{-1}\,2p^{-1}\,(^3P)np$ ($n \geqslant 5$) are included in (c,d), respectively. These spectra are plotted in the Ne^{2+} binding energy scale which is converted from Auger electron energy in the relation of (Ne^{2+} binding energy) = (photon energy–photoelectron energy–Auger electron energy). The transition intensities from the $1s^{-1}$ state to the $2h$ levels, observed by conventional Auger spectroscopy [15,16], are shown in (a) with red bars. The binding energies of the $2h$ and low-lying $3h1e$ levels, as well as the Ne^{3+} threshold, are indicated [19]. The shaded spectra show the contributions from the double Auger decays, which are obtained by the triple coincidences and are scaled by taking into account the known electron detection efficiency. The spectra essentially delineate the distributions of the Ne^{2+} states which are intermediately formed in the cascade double Auger paths, since the contributions from the direct double Auger paths are minor.

into the $Ne^{2+}\,1s^{-1}\,2p^{-1}\,(^{1,3}P)$ states [14], and correspondingly a continuous distribution is seen below a kinetic energy of 80 eV. Resonances due to $1s^{-1}\,2s^{-1}\,(^{1,3}S)ns$ shake-up states are embedded in the shake-off continua [13].

The energy correlation between these photoelectrons and fast Auger electrons in the kinetic energy range of 600–900 eV, extracted from the coincidence dataset, is displayed in Fig. 2(b). Island structures running vertically are observed at the photoelectron energies for the formations of the $1s$ main and remarkable shake-up states, and the vertical cuts of these structures correspond to the coincidence Auger spectra associated with these core-hole states. The black solid curves in Fig. 3 show the coincidence Auger spectra derived for the Auger decays from the $1s^{-1}$, $1s^{-1}\,2p^{-1}\,(^3P)3p$, $1s^{-1}\,2p^{-1}\,(^1P)3p$, and $1s^{-1}\,2p^{-1}\,(^1P)4p$ states. In practice, for better statistics, they are obtained by integrating the coincidence counts over the four photoelectron energy ranges indicated in Fig. 2(a), and thus the spectra in Figs. 3(c) and 3(d) include considerable contributions from the $1s^{-1}\,2p^{-1}\,(^3P)4p$ and $1s^{-1}\,2p^{-1}\,(^3P)np$ ($n \geqslant 5$) states, respectively. Although the spectral resolution ($\sim$15 eV) of these coincidence spectra is insufficient to resolve the individual Ne^{2+} final states, these spectra clearly demonstrate that the formed Ne^{2+} populations are different according to the initial core-hole states.

The coincidence Auger spectrum for the $1s^{-1}$ state [black solid curve in Fig. 3(a)] shows the profile reflecting the Auger transitions into $2h$ states, as can be judged from the comparison with the transition intensities (shown with red bars) observed by conventional Auger spectroscopy [15,16]. Unlike the $1s$ main state, the shake-up states predominantly decay into highly excited states [see Figs. 3(b)–3(d)], where these distributions gradually shift to the higher binding energy side with increase of the energies of the initial shake-up states. These spectral profiles can be interpreted in terms of the dominant formations of $3h1e$ states due to spectator processes. In fact, the first maximum of the distribution in Fig. 3(b) agrees fairly well with the locations of the $2p^{-3}3p$ states which can be formed in the decay of the $1s^{-1}\,2p^{-1}\,(^3P)3p$ shake-up state while keeping the Rydberg electron. The first maxima seen in Figs. 3(c) and 3(d) lie somewhat higher than the locations of such low-lying $3h1e$ states, because, as mentioned above, these spectra include the contributions from higher-lying shake-up states.

In the spectra associated with the shake-up states [Figs. 3(b)–3(d)], formation of $2h$ states due to the participation of the promoted electron is very weakly discernible: For instance, in Fig. 3(b) the contribution from the formation of $2p^{-2}$ states is less than 1% in the total intensity. This fact implies there are unfavorable participant processes in the single Auger decays of the shake-up states. The preference of the spectator processes observed in the present case is much more pronounced than those reported for the single Auger decays from shake-up states in some molecules [5–7]. This is probably because these investigations were made mostly to the shake-up states associated with valence-to-valence promotion and the promoted electron in a valence orbital can participate into the decay process more sizably than the one in a Rydberg orbital does.

B. Double Auger decay

The double Auger decay of each core-hole state can be observed as a triple coincidence of the corresponding photoelectron and two Auger electrons. Figure 4 shows the energy correlations of the two electrons detected in coincidences with the photoelectron for the formation of the $1s^{-1}\,2p^{-1}\,(^3P)3p$ shake-up state. In this two-dimensional plot, because the two Auger electrons for the final production of a Ne^{3+} state share the available energy corresponding to the energy difference between the initial core-hole state and the final Ne^{3+} state, the coincidence yield falls necessarily on the diagonal line defined by $x + y =$ (the available energy). The locations of the diagonal lines for the formations of the $3h$ states in Ne^{3+} are indicated on this map. Intense structures around $(x, y) =$ (800 eV, 0–150 eV), which lie outside of the diagonal lines,

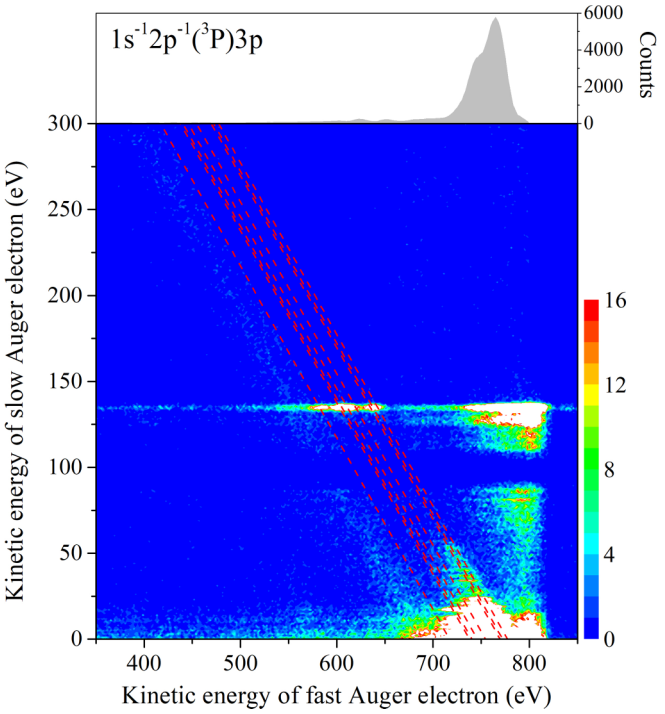

FIG. 4. Two-dimensional map showing energy correlations of the two Auger electrons emitted in the double Auger decay from the $1s^{-1}\,2p^{-1}\,(^3P)3p$ shake-up state. Color represents number of coincidences found in a box of a 1 eV (vertical) × 1.8 eV (horizontal) size. Intense structures around $(x,y) = (800\,\text{eV}, 0\text{–}150\,\text{eV})$ are due to false coincidences including $1s$ photoelectrons and intense single Auger electrons from $1s^{-1}$. The diagonal lines (red broken) indicate the locations of the coincidence yields expected for the final formations of $3h$ states. A blind area arises around $y = 100\,\text{eV}$, because of the overlap with the photoelectron for the formation of the satellite state. The top panel shows the energy distribution of the fast Auger electron, obtained by projecting the coincidence yields on the two-dimensional map toward the x axis. In this projection, the contribution from the false coincidences seen around $(x,y) = (800\,\text{eV}, 0\text{–}150\,\text{eV})$ is excluded.

are due to false coincidences including $1s$ photoelectrons and intense single Auger electrons from the $1s^{-1}$ state. On the other hand, the strong enhancement seen at $y = 136\,\text{eV}$ on the diagonal lines is not due to any false coincidence, even though they are not connected with the decay from the shake-up state. The enhancement is attributed to the double Auger decay from the $1s$ main state, and corresponds to the coincidences between the $1s$ photoelectron and one of the Auger electrons, where the other Auger electron overlaps in kinetic energy with the photoelectron for the formation of the shake-up state.

The direct and cascade paths in the double Auger decays of the shake-up states are expected to produce different specific features along the diagonal lines. The two Auger electrons emitted in the direct path shares the available energy for the formation of the individual Ne^{3+} states, thereby leading to continuous intensities along the diagonal lines. In contrast, each cascade process emits two electrons with discrete kinetic energies defined by the energy levels of the initial Ne^{+}, intermediate Ne^{2+}, and final Ne^{3+} states, and forms an enhancement on the diagonal line for the final Ne^{3+} formation.

Continuous intensities due to the direct double Auger path are hardly discernible in Fig. 4 along the diagonal lines for the formation of the $3h$ states, implying that the direct paths toward these states are unfavorable. On the other hand, one can find a weak diagonal structure around $x + y = 700\,\text{eV}$, which is attributable to the direct double Auger path toward high-lying Ne^{3+} states. Meanwhile, strong enhancements resulting from the cascade double Auger paths are seen below $y < 50\,\text{eV}$ for the $3h$ formations. Here, the energies of the slow Auger electrons define the energy levels of intermediately formed Ne^{2+} states measured from the final Ne^{3+} states. The cascade paths have been partially assigned [9] and include such intermediate states as $2s^{-1}\,2p^{-2}\,3p$ and $2s^{-2}\,2p^{-1}\,3p$.

The top panel of Fig. 4 shows the energy distribution of the fast Auger electron emitted in the double Auger decay of the $1s^{-1}\,2p^{-1}\,(^3P)3p$ shake-up state, obtained by projecting the coincidence yields on the two-dimensional map toward the x axis. In this projection, the contribution from false coincidences seen around $(x,y) = (800\,\text{eV}, 0\text{–}150\,\text{eV})$ is excluded. Since the cascade paths share a considerable fraction of the intensities, the spectrum essentially reflects the distributions of the Ne^{2+} states which are intermediately formed in the cascade double Auger paths. The spectrum, together with spectra obtained in a similar way for the other core-hole states, is shown in Fig. 3 with shaded curves. These may be compared with the total Auger distributions from the individual core-hole states. One finds that essentially all the populations of Ne^{2+} states lying above Ne^{3+} proceed to further electron emission constituting a cascade double Auger path. Considering that these Ne^{2+} states are originally populated by spectator processes in single Auger emission from the core hole, intensities of these cascade double Auger paths stem from the spectator behavior of the Rydberg electron. It is observed that the contribution from double Auger decay increases for higher shake-up states, since the spectator transitions result in higher fractions of the Ne^{2+} populations above the Ne^{3+} threshold.

To reveal the Ne^{3+} states populated by the double Auger decay, the coincidence counts on the two-dimensional map are integrated along the direction for $x + y = \text{const}$. Here, the counts in $y = 130\text{–}140\,\text{eV}$ are masked, in order to exclude the contributions from the $1s$ double Auger decay events. The histogram thus obtained for the $1s^{-1}\,2p^{-1}\,(^3P)3p$ shake-up state, as well as those for other core-hole states, is plotted in Fig. 5 with a black solid curve, as a function of Ne^{3+} binding energy. The spectrum associated with the $1s^{-1}$ state shows three broad structures attributable to $2p^{-3}$, $2s^{-1}\,2p^{-2}$, and $2s^{-2}\,2p^{-1}$ of Ne^{3+}. Predominant formations of these $3h$ states are also presented in the spectra associated with the shake-up states, where the formations of the $2p^{-3}$ states are enhanced. While the locations of low-lying $4h1e$ states are indicated in Figs. 5(b)–5(d) with vertical bars, pronounced intensities ascribable to their formations are not identified in these spectra. This observation implies that, in contrast to the single Auger decays, the Auger final states without the Rydberg electrons are favorably populated in the overall double Auger decays of the shake-up states. Here, the net Ne^{3+} distributions resulting from simultaneous emissions of two Auger electrons are hidden behind large contributions from the cascade paths.

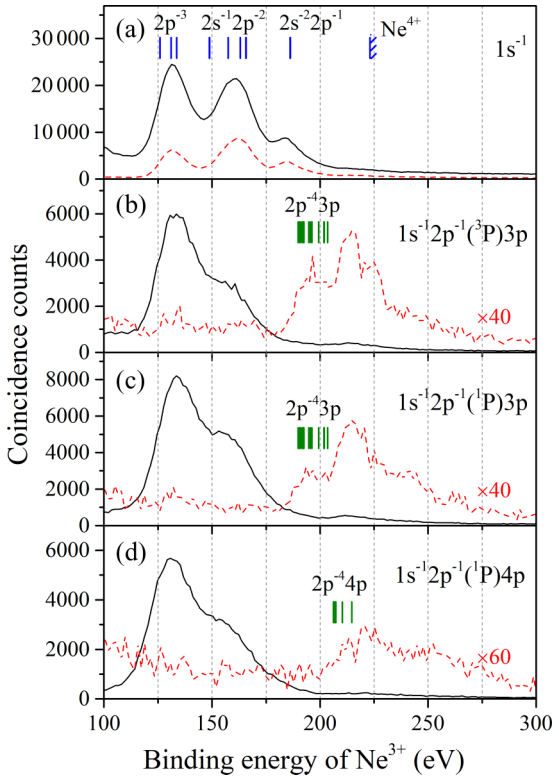

FIG. 5. Spectra showing the populations of the Ne^{3+} states formed by the double Auger decays from (a) $1s^{-1}$, (b) $1s^{-1}\,2p^{-1}\,(^3P)3p$, (c) $1s^{-1}\,2p^{-1}\,(^1P)3p$, and (d) $1s^{-1}\,2p^{-1}\,(^1P)4p$. Contributions from $1s^{-1}\,2p^{-1}\,(^3P)4p$ and $1s^{-1}\,2p^{-1}\,(^3P)np$ $(n \geqslant 5)$ are included in (c,d), respectively. While the black solid curves are obtained for the whole processes of the double Auger decays, the red broken curves are deduced by eliminating the events including a slow electron with a kinetic energy below 50 eV and thus represent the Ne^{3+} populations resulting from the direct double Auger paths. These spectra are plotted in the Ne^{3+} binding energy scale which is converted from sum of the energies of two Auger electrons, in the relation of (Ne^{3+} binding energy) = (photon energy)–(photoelectron energy)–(sum of the energies of two Auger electrons). The binding energies of the $3h$ and low-lying $4h1e$ levels, as well as the Ne^{4+} threshold, are indicated [19].

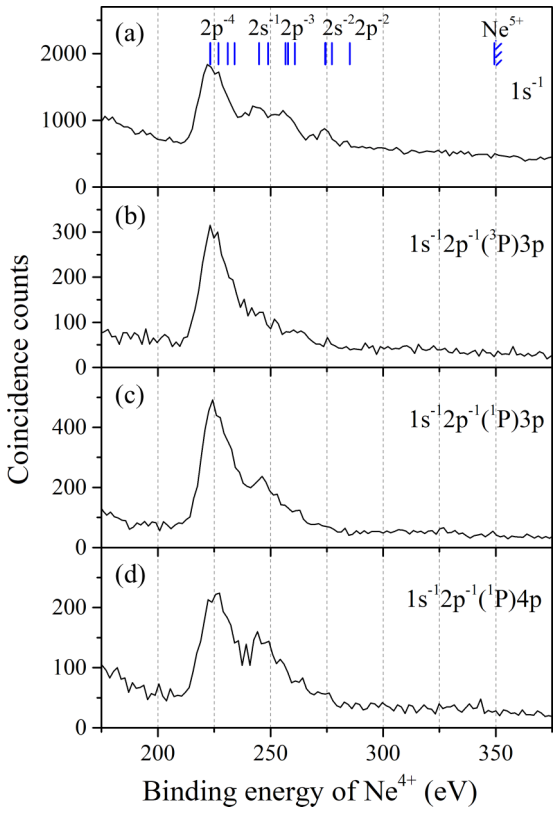

FIG. 6. Spectra showing the populations of the Ne^{4+} states formed by the triple Auger decays from (a) $1s^{-1}$, (b) $1s^{-1}\,2p^{-1}\,(^3P)3p$, (c) $1s^{-1}\,2p^{-1}\,(^1P)3p$, and (d) $1s^{-1}\,2p^{-1}\,(^1P)4p$. Contributions from $1s^{-1}\,2p^{-1}\,(^3P)4p$ and $1s^{-1}\,2p^{-1}\,(^3P)np$ $(n \geqslant 5)$ are included in (c,d), respectively. These spectra are plotted in the Ne^{4+} binding energy scale which is converted from sum of the energies of two Auger electrons, in the relation of (Ne^{4+} binding energy) = (photon energy)−(photoelectron energy)–(sum of the energies of three Auger electrons). The binding energies of the $4h$ levels, as well as the Ne^{5+} threshold, are indicated [19].

The coincidence events for the cascade path in the double Auger decay from the $1s^{-1}\,2p^{-1}\,(^3P)3p$ shake-up state are remarkably seen in Fig. 4 only below $y = 50$ eV, and similar features are observed also for the other shake-up states. The contributions from the cascade paths can thus be effectively removed by eliminating the events including such a slow Auger electron. The red broken curves in Fig. 5 are obtained by eliminating the events including a slow electron with a kinetic energy below 50 eV, and thus represent the Ne^{3+} populations resulting from the direct double Auger paths. Here, the spectral profiles do not essentially change even if the kinetic-energy mask is extended toward higher kinetic energy. Note that these spectra exhibit the contributions from a part of the direct double Auger processes whose energy distributions continue toward zero kinetic energy, and thus may be somewhat deformed from the Ne^{3+} distributions associated with the whole direct paths.

The red broken curves in Figs. 5(b)–5(d) show sizable formations of highly excited states in the binding energy range of 180–250 eV. These high-lying states are attributable to the $4h1e$ states resulting from the spectator behavior of the Rydberg electrons in the direct double Auger paths, because the starts of the structures show reasonable agreements with the locations of low-lying $4h1e$ states. Formation of $3h$ states disappears in these spectra, implying that the participation of the Rydberg electron is unfavored in the direct double Auger decay. Thus, similar to the single Auger decays, the Rydberg electron predominantly behaves as a spectator on the simultaneous emissions of the two Auger electrons. Even assuming that all the intensities of the black solid spectra in the $4h1e$ regions were ascribed to the direct double Auger paths, the contributions from the direct paths share only 8%–10% in the total double Auger decays.

C. Triple Auger decay

Weak but true quadruple coincidence signals for the triple Auger decays from the shake-up states can be recognized in the coincidence dataset. Figure 6 shows the spectra of the energy sums of the three Auger electrons observed in coincidence with the photoelectron for the formation of the individual core-hole

TABLE I. Branching ratios of product ions formed from individual core-hole states, estimated with the coincidence counts and the electron detection efficiency. The values for $1s^{-1}\,2p^{-1}\,(^1P)3p$ and $1s^{-1}\,2p^{-1}\,(^1P)4p$ include contributions from $1s^{-1}\,2p^{-1}\,(^3P)4p$ and $1s^{-1}\,2p^{-1}\,(^3P)np$ ($n \geqslant 5$), respectively. The formation of Ne^+ is unobservable with the present method. The values reported by Kanngießer *et al.* for the $1s^{-1}$ state [18], normalized as the Ne^{2+} value to be unity, are compared.

Ion charge state	$1s^{-1}$	$1s^{-1}$ [18]	$1s^{-1}2p^{-1}$ $(^3P)3p$	$1s^{-1}2p^{-1}$ $(^1P)3p$	$1s^{-1}2p^{-1}$ $(^1P)4p$
Ne^+		0.0010			
Ne^{2+}	1	1	1	1	1
Ne^{3+}	0.05	0.0644	0.57	0.65	1.52
Ne^{4+}	0.004	0.0041	0.03	0.04	0.06

states. Similar profiles are exhibited in these spectra, and can be interpreted as the formations of the four-hole ($4h$) states of Ne^{4+}. As for the triple Auger decay from the $1s^{-1}$ state, an important contribution from the cascade path consisting of direct double Auger decay into highly excited Ne^{3+} and the subsequent single electron emissions has been identified in the energy correlations among the three Auger electrons [17]. Poor statistics of the quadruple coincidence events associated with the shake-up states does not allow us to judge if such cascade pathway is important also in the triple Auger decay of the shake-up states. However, this cascade pathway can be significant in the triple Auger decays, considering that highly excited Ne^{3+} states lying above the Ne^{4+} threshold are sizably populated by the spectator transition in the direct double Auger paths from the shake-up states (see the red broken curves in Fig. 5).

D. Ion branching ratio

Branching ratios of product ions formed from the shake-up states, as well as that from the $1s^{-1}$ state, are estimated with the coincidence counts and the electron detection efficiency. They are given in Table I, and are compared with the ion branching ratio obtained for the $1s^{-1}$ state by a photoelectron-ion coincidence method [18]. The present values for the $1s^{-1}$ state agree well with the high-accuracy data by the photoelectron-ion coincidence method, assuring high reliability of the values derived in this study for the shake-up states. The branching ratios of Ne^{3+} and Ne^{4+} ions are one order of magnitude higher for the shake-up states than for the $1s^{-1}$ state. Here, increases of the branching ratios of these ions are observed for higher shake-up states. The enhancements of the formations of Ne^{3+} and Ne^{4+} from the shake-up states are due to the cascade paths via high-lying intermediate states favorably populated by the spectator processes, as the present multielectron coincidence study has revealed.

IV. CONCLUSIONS

A comprehensive investigation of the Auger decay processes from $1s$ shake-up states of Ne has been performed by multielectron coincidence spectroscopy. The single Auger decays result in dominant formation of $3h1e$ states, due to the retention of the Rydberg electron promoted in the initial ionization step. Some of the $3h1e$ states (for example, $2s^{-1}\,2p^{-2}\,3p$ and $2s^{-2}\,2p^{-1}\,3p$) lie above the Ne^{3+} threshold, and their decay, which involves the participation of the Rydberg electron, constitutes the second step in the cascade path of the double Auger decay. In the direct double Auger paths, the spectator processes producing $4h1e$ states are predominant. Consequently, the Rydberg electron promoted in the photoionization step behaves almost exclusively as a spectator in the first step of all decay paths of the core hole. Important participation of the Rydberg electron occurs only after the filling of the core hole, when the states formed by the core-hole decay are excited enough to emit another electron.

ACKNOWLEDGMENTS

The authors are grateful to the Photon Factory staff for the stable operation of the PF ring. We thank Ronald McCarroll for a careful reading of the manuscript. Financial support from JSPS (Grant No. 18540399) and CNRS is acknowledged. This work was performed with the approval of the Photon Factory Program Advisory Committee (Proposals No. 2006G230 and No. 2008G519).

[1] K. Siegbahn, C. Nordling, G. Johansson, J. Hedman, P. F. Hedén, K. Hamrin, U. Gelius, T. Bergmark, L. O. Werme, R. Manne, and Y. Baer, *ESCA Applied to Free Molecules* (North-Holland, Amsterdam, 1969).

[2] T. Åberg, Phys. Rev. **156**, 35 (1967).

[3] M. Nakano, Y. Hikosaka, P. Lablanquie, F. Penent, S.-M. Huttula, I. H. Suzuki, K. Soejima, N. Kouchi, and K. Ito, Phys. Rev. A **85**, 043405 (2012).

[4] M. Neeb, J. E. Rubensson, M. Biermann, and W. Eberhardt, J. Phys. B **29**, 4381 (1996).

[5] T. Kaneyasu, Y. Hikosaka, E. Shigemasa, P. Lablanquie, F. Penent, and K. Ito, J. Phys. B **41**, 135101 (2008).

[6] S. Zagorodskikh, V. Zhaunerchyk, M. Mucke, J. H. D. Eland, R. J. Squibb, L. Karlsson, P. Linusson, and R. Feifel, Chem. Phys. **463**, 159 (2015).

[7] T. Kaneyasu, T. Odagiri, M. Nakagawa, R. Mashiko, H. Tanaka, J. Adachi, and Y. Hikosaka, J. Chem. Phys. **147**, 104304 (2017).

[8] J. Keskinen, P. Lablanquie, F. Penent, J. Palaudoux, L. Andric, D. Cubaynes, J.-M. Bizau, M. Huttula, and K. Jänkälä, Phys. Rev. A **95**, 043402 (2017).

[9] Y. Hikosaka, T. Aoto, P. Lablanquie, F. Penent, E. Shigemasa, and K. Ito, J. Phys. B, **39**, 3457 (2006).

[10] M. Leväsalmi, H. Aksela, and S. Aksela, Phys. Scr. **T41**, 119 (1992).

[11] K. Ito, F. Penent, Y. Hikosaka, E. Shigemasa, I. H. Suzuki, J. H. D. Eland, and P. Lablanquie, Rev. Sci. Instrum. **80**, 123101 (2009).

[12] J. H. D. Eland, O. Vieuxmaire, T. Kinugawa, P. Lablanquie, R. I. Hall, and F. Penent, Phys. Rev. Lett. **90**, 053003 (2003).

[13] N. Mårtensson, S. Svensson, and U. Gelius, J. Phys. B **20**, 6243 (1987).
[14] Y. Hikosaka, T. Aoto, P. Lablanquie, F. Penent, E. Shigemasa, and K. Ito, Phys. Rev. Lett. **97**, 053003 (2006).
[15] M. O. Krause, T. A. Carlson, and W. E. Moddeman, J. Phys. (Paris) **32**, C4-139 (1971).
[16] A. Albiez, M. Thoma, W. Weber, and W. Mehlhorn, Z. Phys. D **16**, 97 (1990).
[17] Y. Hikosaka, T. Kaneyasu, P. Lablanquie, F. Penent, E. Shigemasa, and K. Ito, Phys. Rev. A **92**, 033413 (2015).
[18] B. Kanngießer, M. Jainz, S. Brünken, W. Benten, Ch. Gerth, K. Godehusen, K. Tiedtke, P. van Kampen, A. Tutay, P. Zimmermann, V. F. Demekhin, and A. G. Kochur, Phys. Rev. A **62**, 014702 (2000).
[19] NIST Atomic Spectra Database (ver. 5.3), available at http://physics.nist.gov/asd.